Part II: Diffraction from Two-Dimensional Cholera Toxin Crystals Bound to Their Receptors in a Lipid Monolayer

C. E. Miller,* J. Majewski,* E. B. Watkins,*¶ M. Weygand,† and T. L. Kuhl‡§

*Manuel Lujan Neutron Scattering Center, Los Alamos National Laboratory, Los Alamos, New Mexico; †Department of Physics, Carnegie Mellon University, Pittsburgh, Pennsylvania; ‡Department of Chemical Engineering and Material Science, University of California, Davis, California; §Department of Biomedical Engineering, University of California, Davis, California; and ¶Biophysics Graduate Group, University of California, Davis, California

ABSTRACT The structure of cholera toxin ($CTAB_5$) bound to its putative ganglioside receptor, galactosyl-*N*-acetylgalactosaminyl (*N*-acetyl-neuraminyl) galactosylglucosylceramide (GM_1), in a lipid monolayer at the air-water interface has been studied utilizing grazing incidence x-ray diffraction. Cholera toxin is one of very few proteins to be crystallized in two dimensions and characterized in a fully hydrated state. The observed grazing incidence x-ray diffraction Bragg peaks indicated cholera toxin was ordered in a hexagonal lattice and the order extended 600–800 Å. The pentameric binding portion of cholera toxin (CTB_5) improved in-plane ordering over the full toxin ($CTAB_5$) especially at low pH. Disulfide bond reduction (activation of the full toxin) also increased the protein layer ordering. These findings are consistent with A-subunit flexibility and motion, which cause packing inefficiencies and greater disorder of the protein layer. Corroborative out-of-plane diffraction (Bragg rod) analysis indicated that the scattering units in the cholera layer with $CTAB_5$ shortened after disulfide bond reduction of the A subunit. These studies, together with Part I results, revealed key changes in the structure of the cholera toxin-lipid system under different pH conditions.

INTRODUCTION

Protein structure determination by classical x-ray crystallography requires three-dimensional crystals that are difficult to obtain for many proteins and especially integral membrane proteins. One possible alternative is to grow two-dimensional (2D) crystals by assembling proteins under ligand-lipid monolayers at the surface of water (1–7). Such 2D protein crystals can be studied using grazing incidence x-ray diffraction (GIXD), a popular surface sensitive technique for studying the lateral structure of surfactant molecules at the air-water interface (8,9). GIXD can be conducted under physiological conditions and does not require staining, high vacuum, low temperatures, fast freezing, or complicated sample preparation. The technique is complementary to electron crystallography but of more limited resolution.

One obstacle in using GIXD to study protein monolayers at the air-water interface is that few proteins can be assembled with sufficiently high coverage to form ordered 2D structures. Haas and coworkers were the first to demonstrate GIXD from a 2D protein layer using the streptavidin-biotin system (1). Verclas and coworkers investigated bacteriorhodopsin (purple membrane) (3,4), while Lösche and coworkers have investigated the coupling of protein sheet crystals (S-layers) to phospholipid monolayers (5–7). Similar to the studies here, Lenne et al. utilized GIXD to characterize streptavidin, annexin V, and the transcription factor HupR while bound to their associated lipid-anchored receptor (2). They also studied cholera toxin but did not observe a GIXD signal from the 2D film. In this study, we present, to our knowledge, the first successful GIXD investigation of cholera toxin bound to a lipid monolayer.

Previously, electron microscopy (EM) has been used to structurally characterize the arrangement of CTB_5 bound to a lipid membrane. The results of Ludwig and coworkers revealed a ring structure with a central hole diameter of 20 Å and an outer ring diameter of 60 Å, consistent with the pentameric structure of the B_5 subunit flat on the membrane surface (10). Also observed was the coexistence of two different protein crystal lattices 1), a rectangular unit cell ($a = 120$ Å, $b = 131$ Å, $\gamma = 90°$) with electron density distribution revealing pentameric units; and 2), a hexagonal unit cell ($a_{hex} = 68$Å), which represented a disordered liquid crystalline form with rotational averaging about the pentamer's 5-fold axis. The proportion of the two crystal forms varied with no discernible dependence on pH, ionic strength, time, or temperature. Subsequent, higher resolution measurements revealed that the pentameric motif had an outer diameter of 67 Å and central pore diameter of 12 Å (11). The close correspondence in structural dimensions obtained via subsequent three-dimensional (3D) x-ray crystallography (12) and EM, between the soluble and membrane-bound forms of CTB_5, suggested that only minor structural changes occurred to the protein when binding to its receptor, galactosyl-*N*-acetylgalactosaminyl (*N*-acetyl-neuraminyl) galactosylglucosylceramide (GM_1).

More recently, EM was used to study 2D crystals of $CTAB_5$ bound to a single lipid monolayer (13). Structure determination revealed the B_5 ring on the membrane surface, but only a third of the A subunit mass was visible in the center of the ring. It was proposed that the remaining mass of the A

Submitted August 28, 2007, and accepted for publication February 12, 2008.

Address reprint requests to Jarek P. Majewski, Los Alamos National Laboratory, Manuel Lujan Neutron Scattering Center, LANSCE-12, Los Alamos National Laboratory, Los Alamos, NM 87545. Tel.: 505–667–8840; E-mail: jarek@lanl.gov.

Editor: Thomas J. McIntosh.

0006-3495/08/07/641/07 $2.00

doi: 10.1529/biophysj.107.120808

subunit penetrated the hydrophobic interior of the membrane. Another possibility was that conformational disorder of the A subunit diminished its scattering contribution. Moreover, activation of the toxin by addition of dithiothreitol, (DTT) revealed a protein structure that appeared intermediate between those of CTB_5 and the complete toxin. Based on these EM images, it was concluded that activation dissociated the A1 fragment from the central channel (13). As we will discuss, our GIXD investigations of cholera toxin crystals bound to lipid monolayers at the air-water interface reveal similar structural changes after activation.

To model the cellular membrane, we used a system consisting of a two-component lipid monolayer at the air-water interface, where one component was cholera's receptor, ganglioside GM_1. The other component, gel-phase 1, 2-dipalmitoyl-*sn*-glycero-3-phosphoethanolamine (DPPE), has previously been established to mix well with GM_1 and acts as the lipid matrix (14). Using x-ray scattering, we investigated the interactions between these model membranes and cholera toxin at pH = 8, which represents the environment exterior to the cell, and pH = 5, which represents the low endosomal pH that the toxin would be subjected to after endocytosis. In Part I of this work (14) we reported the x-ray reflectivity of the cholera-membrane system and the GIXD from the lipid monolayer. Here in Part II, we address the GIXD from the bound protein layer nucleated under the lipid monolayer, including measurements of the 2D protein crystal lattice, the orientation and tilt angle of the protein relative to the membrane plane, and structural changes to $CTAB_5$ after enzymatic activation.

MATERIALS AND METHODS

All lipid monolayers were composed of 80:20 mol % of DPPE:GM_1. More complete details are provided in Part I (14). Unless otherwise noted, the monolayer's molar composition, surface pressure of 20 mN/m, and temperature of 23°C were held constant throughout each experiment. Under these conditions, the lipid monolayer was predominately in the gel-phase and had significant in-plane ordering enabling GIXD measurements (discussed in Part I). Cholera solution was injected into the subphase (under the monolayer) to a final concentration of ~4 mg/L, and the subphase was continuously circulated by a peristaltic pump at a rate of ~8 mL/min. Cholera toxin was allowed to incubate for 1–3 h before scanning. To ''activate'' cholera toxin, we used DTT (Cleland's reagent) injected into subphase to yield a concentration of 4.6 mg/mL to reduce the disulfide bond (Cys-187=Cys-199) between the A1 and A2 subunit. DTT is frequently used to reduce protein disulfide bonds though it is unable to reduce buried (solvent-inaccessible) disulfide bonds. DTT was also allowed to incubate for 1–3 h before scanning. Unless otherwise noted, the same lipid monolayer was used without respreading for a sequence of experiments involving protein injection ($CTAB_5$ or CTB_5) and its activation. The theory of GIXD has been presented in great detail elsewhere (8,9,15,16).

RESULTS AND DISCUSSION

GIXD analysis (pH = 8)

GIXD measurements provide in-plane structural information of the ordered, diffracting portion of the monolayer-protein system. In general, the diffraction from the lipid-protein

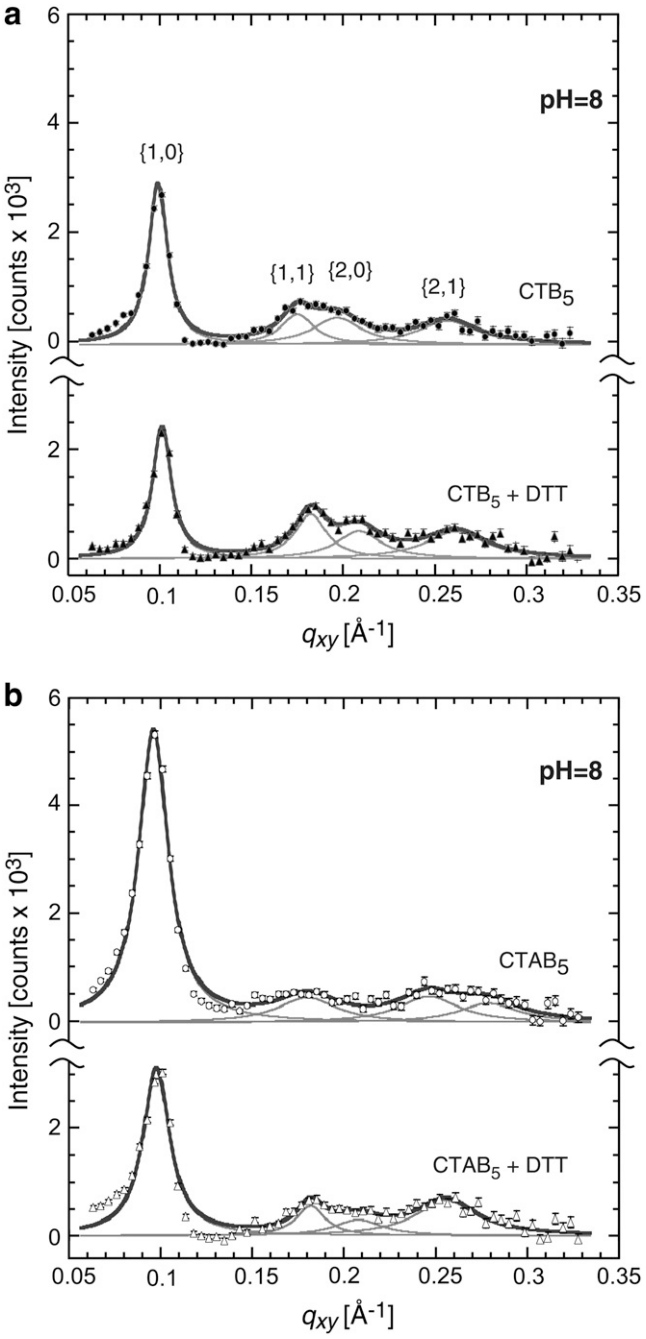

FIGURE 1 GIXD Bragg peaks obtained for layers of CTB_5 and $CTAB_5$ at pH = 8. The protein crystals nucleated under the DPPE:GM1 monolayer forming an ordered 2D protein monolayer with hexagonal packing. (*a*) Bragg peaks from CTB_5 and CTB_5 + DTT. Miller indices {h, k} of the observed peaks are indicated. Bragg peaks were integrated over the q_z region (–0.05 to 0.2 $Å^{-1}$). Peaks were fitted (*solid lines*) using Lorenzian curves (see Table 1 for details). (*b*) Bragg peaks from $CTAB_5$ and $CTAB_5$ + DTT. Intensities and positions of the Bragg peaks (especially higher order) in the case of $CTAB_5$ had larger uncertainties due to weaker in-plane ordering and a higher incoherent background contribution due to the A subunit.

system was observed only in two regions; a low q_{xy} region from 0.08 to 0.30 $Å^{-1}$ corresponding to real-space d-spacings of ~80 to ~20 Å from the 2D ordering of the cholera protein layer, and a q_{xy} region from ~1.3 to ~1.6 $Å^{-1}$ corresponding to d-spacings of ~4.4 to ~4.2 Å from diffraction of the alkyl tails. Here we discuss diffraction from the cholera protein layer. In Part I reflectivity measurements of the lipid-protein system and diffraction from the lipid monolayer were reported (14). Based on reflectivity measurements, which provide an average electron density profile normal to the air-water interface, the experimentally obtained protein area coverage varied between 49–62% of the lipid monolayer.

Diffraction from the protein layer: Bragg peaks

Measurements of the diffraction patterns obtained at pH = 8 from the whole toxin, $CTAB_5$, the binding portion, CTB_5, and both proteins after the addition of a strong reducing agent, DTT, are shown in Fig. 1 and summarized in Table 1. In all cases, protein crystals formed under the lipid monolayer, and their diffraction yielded one strong peak and three weak peaks. Measurements of the low q_{xy} range (0.08 $Å^{-1}$ to 0.35 $Å^{-1}$) were challenging due to proximity to the direct beam and the diffraction peaks from the Kapton windows, which complicated background subtraction. Therefore, confidence in the intensities and positions of higher-order reflections are less certain. After background subtraction, the Bragg peaks were obtained by integrating over the region ($-0.05\ Å^{-1} \le q_z \le 0.2\ Å^{-1}$). The observed GIXD Bragg peaks indicated packing of the proteins in hexagonal 2D unit cells. Miller indices {h, k} of the observed peaks are indicated in Fig. 1 *a*.

For a 2D hexagonal unit cell with dimension a_{hex}, the spacings between {h, k} planes are described by Eq. 1:

$$1/d_{hk}^2 = 4(h^2 + hk + k^2)/3a_{hex}^2. \quad (1)$$

Based on the peak positions and Eq. 1, a least-square fit was applied to obtain the hexagonal unit cell parameter a_{hex}. Taking into account the error bars of these measurements, there was no significant change in the unit cell parameter a_{hex} between the proteins with or without DTT yielding 73.7 ± 1.0 Å for CTB_5, 71.3 ± 2.0 Å for CTB_5 + DTT, 71.4 ± 3.5 Å for $CTAB_5$, and 72.3 ± 3.0 Å for $CTAB_5$ + DTT.

Compared to CTB_5, the {1,0} peak of $CTAB_5$ had a higher intensity because of additional electrons from the A subunit (Fig. 1 *b*) and/or differences in toxin occupancy. Activation of $CTAB_5$ by DTT decreased the intensity of the {1,0} peak consistent with increased conformational disorder from disulfide reduction of the A subunit. In addition, the visibility of the higher-order Bragg peaks became more pronounced indicating better in-plane order of the remaining toxin. Similar behavior was also observed at pH = 5 comparing $CTAB_5$ with $CTAB_5$ + DTT.

Intrinsic full width at half maxima (FWHM) and corresponding lateral coherence lengths, L_{xy} (approximate dimension of the ordered domains), were obtained as described in Part I using the equations:

$$FWHM_{intrinsic}(q_{xy}) = [FWHM_{meas}(q_{xy})^2 - FWHM_{resol}(q_{xy})^2]^{1/2}$$
$$\text{and} \quad L_{xy} \approx 0.9[2\pi/FWHM_{intrinsic}(q_{xy})]\{h,k\} \quad (17).$$

Lateral coherence lengths for each peak are enumerated in Table 1. Due to the uncertainty of the FWHM of the higher-order peaks, only the {1,0} reflection was analyzed in detail. The lateral coherence length (L_{10}) for CTB_5 was significantly larger than L_{10} for $CTAB_5$ (~600 Å vs. ~300 Å). After activation of $CTAB_5$ with DTT, the Bragg peaks were more similar to that of CTB_5, suggest that some of the reduced A1 subunits may not have been contributing to the scattering (a small increase in L_{10} was observed indicative of an enhancement in in-plane order).

TABLE 1 Protein layer in-plane Bragg peaks of CTB_5 and $CTAB_5$ protein layers

	pH = 8													
	Observed d-spacings ± 0.5 (Å)				Integrated intensity* ± 1.0				Area per molecule ± 100 ($Å^2$)	Hex unit cell a_{hex} (Å)	In-plane coherence length, L(Å) ± 50 Å			
Composition	{1,0}	{1,1}	{2,0}	{2,1}	{1,0}	{1,1}	{2,0}	{2,1}			{1,0}	{1,1}	{2,0}	{2,1}
CTB_5	63.5	35.9	32.0	24.4	57	19	25	27	4708	73.7 ± 1	623	283	180	†
CTB_5 + DTT	62.1	34.5	30.1	22.5	46	27	24	32	4407	71.3 ± 2	634	294	198	†
$CTAB_5$	65.4	34.9	25.5	22.5	165	29	31	23	4413	71.4 ± 3.5	323	†	†	†
$CTAB_5$ + DTT	64.4	34.5	30.2	24.6	86	17	15	42	4531	72.3 ± 3	366	332	186	†
	pH = 5													
CTB_5	61.6	34.9	30.9	24.1	54	27	18	32	4504	72.1 ± 1	711	264	323	†
CTB_5 + DTT	60.7	34.2	30.2	23.9	41	34	24	39	4372	71.1 ± 2	805	197	280	†
$CTAB_5$	60.9	35.2	31.3	23.5	134	12	2	34	4434	71.6 ± 1	480	283	†	†
$CTAB_5$ + DTT	60.7	34.8	30.3	23.5	78	6	13	44	4339	70.8 ± 1	590	633	208	†

*Intensities in arbitrary units
†Impossible to get reliable data

Diffraction from the protein layer: Bragg rods

Bragg rod profiles at pH = 8 (Fig. 2) were produced by integrating through the 0.08 $Å^{-1} \leq q_{xy} \leq 0.12$ $Å^{-1}$ region of the {1,0} Bragg peak. It was not possible to reliably extract the Bragg rods of the higher-order reflections. Due to the 2D nature of the system, Bragg rods are extended in q_z space and the scattered intensity along q_z is modulated by the form factor of the scattering units. Models based on the molecular 3D crystal structure taken from the protein database (1fgb, 1xtc) were constructed and compared to the data. Unfortunately, when modeling the Bragg rods by a single molecular layer, no orientations (tilts and translations within the unit cell) were able to reproduce the experimental data.

To glean insight into the structure of the scattering unit, we used a cylindrical object to model the Bragg rod profiles. Parameters corresponding to the cylinder's height, radius, tilt angle from the surface normal, and root mean-square molecular displacement (Debye-Waller (DW) factor) normal to the interface were adjusted using a Levenberg-Marquardt least-squares fitting algorithm to obtain the best possible fit. All structural parameters of the cholera layer obtained from this analysis are reported in Table 2. For CTB_5 the radius of the cylinder obtained from least-square refinement was 37 Å, which matches well with $\sim a_{hex}/2$ obtained from the Bragg peak analysis. The radius of the cylinder was slightly larger than the radius of 31 Å reported from the 3D crystal structure (12) suggesting that the cholera molecules were not close packed. Surprisingly, the height of the scattering cylinder obtained from fitting the data was 57 Å, too large to be accounted for solely by the B_5 subunit (32 Å from the 3D crystal structure), yet too small for a CTB_5 dimer. Moreover, a protein dimer layer (normal to the interface) was not observed by reflectivity measurements (14). To account for this height, we hypothesize that these scattering cylinders represent the CTB_5 protein and a correlated group of lipids constrained by bound GM_1 molecules in the toxin's five receptor binding sites (Fig. 2 *b*). The fitted cylinder tilt of 38° is also consistent with the tilt of the lipid molecules in the region where toxin was bound (phase 2) (results obtained from GIXD analysis in Part I). Since one GM_1 lipid molecule bound to each B subunit of cholera is expected, it is reasonable to assume that the cholera molecule lies parallel to the monolayer surface. EM measurements also show this orientation (10,11,13). As a result, any tilt angle of the cylinder is likely due to the tilt of the lipid molecules. Aside from any model, the Bragg rod data (Fig. 2 *a*) has an intensity maximum off the horizon ($q_z \sim 0.12$ $Å^{-1}$), and therefore the scattering entity is tilted from the surface normal. All attempts to model a height corresponding to the dimensions of the CTB_5 protein alone resulted in an intensity maximum at a smaller q_z value than the measured data. Therefore, any model required an object longer than the protein alone. Although a scattering entity of protein with a lipid ''corona'' connected to it is unconventional, contrast in electron density

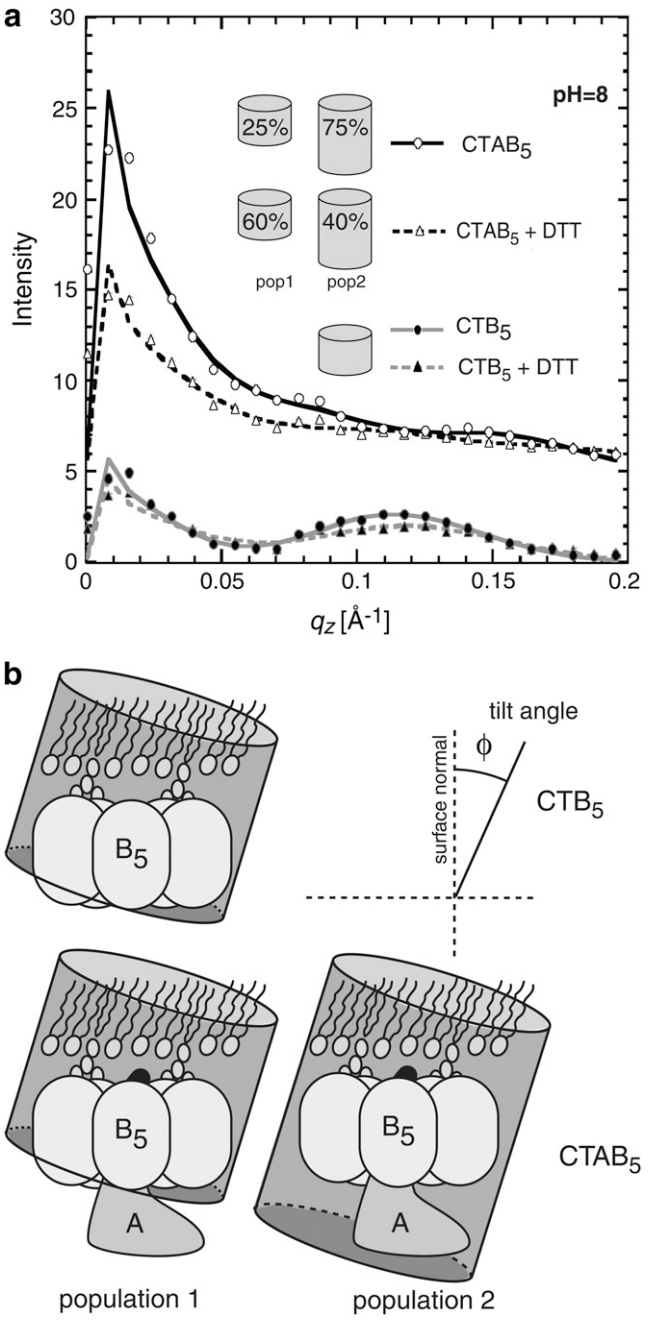

FIGURE 2 (*a*) Bragg rod profiles corresponding to scattering from the cholera protein layer at pH = 8. Rods were produced by integrating through the 0.08 $Å^{-1} \leq q_{xy} \leq 0.12$ $Å^{-1}$ region of the {1,0} Bragg peaks in Fig. 1. The profiles corresponding to $CTAB_5$ have been offset by 6 for clarity. The sharp peak at $q_{xy} \sim 0.01$ $Å^{-1}$ is the Vineyard-Yoneda peak (18). Error bars are smaller than the symbol size. Lines are fits to the profiles based on cylinders shown in *b*. (*b*) Schematic representation of the cylindrical objects used to approximate the scattering units. Structural parameters such as the cylinder's height, radius, and tilt angle of the cholera molecules are reported in Table 2. In the case of $CTAB_5$, two populations of cylinders were used to fit the data. After activation of $CTAB_5$ there was a shift from ~75% to ~40% for population 2.

TABLE 2 Protein layer out-of-plane Bragg rods of CTB_5 and $CTAB_5$ protein layers

pH = 8					
	Height ± 1.0 (Å)	Radius ± 0.5 (Å)	Tilt angle ± 2.0 (degrees)	σ ± 1.0 (Å)	χ^2
CTB_5	57.1	37.0	38.2	1	3.0
CTB_5 + DTT	52.9	36.3	39.1	1	2.6
$CTAB_5$ (pop 1) 25 ± 1%	44.9	32.3	42.5	5	10.4
(pop 2) 75 ± 1%	81.1		40.7		
$CTAB_5$ + DTT (pop 1) 60 ±1%	42.9	32.8	31.8	1	6.0
(pop 2) 40 ± 1%	61.3		49.6		
pH = 5					
	Height ± 1.0 (Å)	Radius ± 0.5 (Å)	Tilt angle ± 2.0 (degrees)	σ ± 1.0 (Å)	χ^2
CTB_5	55.3	36.7	37.6	1	2.4
CTB_5 + DTT	51.7	36.3	37.0	1	2.5
$CTAB_5$ (pop 1) 19 ± 1%	43.1	33.3	39.1	5	8.2
(pop 2) 81 ± 1%	82.6		41.9		
$CTAB_5$ + DTT (pop 1) 40 ± 1%	43.4	31.9	34.5	1	6.3
(pop 2) 60 ± 1%	76.1		48.1		

σ is the DW factor or root mean-square molecular displacement normal to the interface. Tilt direction was defined to be toward the nearest neighbor. Fitting the azimuthal tilt direction did not significantly improve χ^2.

between the corona lipids and their neighboring lipids is consistent with the 17% increase in area per molecule as shown by GIXD analysis from scattering of the lipid tails (Part I (14)).

With the addition of DTT, there was a slight decrease in the height of the cylinder. This reduction in height is consistent with a few angstroms decrease in the thickness of the lipid tails seen in the reflectivity results and is further evidence of a single layer of cholera molecules. The same trend was observed with $CTAB_5$ before and after enzymatic activation.

The Bragg rod scattering from $CTAB_5$ could not be modeled using a single population of tilted cylinders. Instead, two populations of tilted cylinders were required (Fig. 2 *b*). From least-square fitting of the intensity distribution along the Bragg rod, population 1 had a vertical height of ~45 Å and population 2 had a height of ~81 Å. We hypothesize that the short cylinder (population 1) represents the coherently scattering combination of only the B_5 pentamer and the lipid molecules constrained on top of it, similar to the single population in the case of CTB_5 (~57 Å vs. ~45 Å). In this population the A subunit has significant freedom of motion relative to the B_5 subunit and does not contribute to the coherent scattering from the CTB_5 pentamer and attached lipid molecules. On the other hand, the taller cylinders used to model population 2 represent scattering from $CTAB_5$ molecules whose A-subunits are oriented in a way that coherently contributes to the overall scattering. Before activation with DTT, our models indicated 25% occupancy of population 1 and 75% occupancy of population 2. After activation with DTT, the occupancy was 60% for population 1 and 40% for population 2. This change is consistent with a significant fraction of the A1 subunits not contributing to the scattering because of a decrease in their order. The root mean-square molecular displacement normal to the interface (DW factor, σ) of the protein layer also decreased from 5 Å to 1 Å after activation, which is indicative of a less disordered layer similar to the CTB_5 case.

GIXD analysis (pH = 5)

Diffraction from the protein layer: Bragg peaks

The diffraction pattern obtained for the cholera protein layer at pH = 5 and 20 mN/m is shown in Fig. 3 and summarized in Table 1. Similar to pH = 8, one strong peak and three weak peaks were distinguishable, and their positions indicated packing of the proteins in a hexagonal 2D unit cell. The a_{hex} parameters obtained from least-squares refinement were 72.1 ± 1 Å for CTB_5, 71.1 ± 2 Å for CTB_5 + DTT, 71.6 ± 1 Å for $CTAB_5$, and 70.8 ± 1 Å for $CTAB_5$ + DTT, which again match well with the 3D crystal structure and EM measurements. The {1,0} peak of $CTAB_5$ (Fig. 3 *b*) was more intense at pH = 5 then pH = 8. The higher-order Bragg peaks also became more visible after activation with DTT, especially in the case of $CTAB_5$, as evidenced by an increase in the L_{10} in-plane coherence lengths (Table 1). The Bragg peaks of $CTAB_5$ + DTT were again more similar to that of CTB_5.

Diffraction from the protein layer: Bragg rods

Bragg rod profiles of the {1,0} Bragg peak at pH = 5 are shown in Fig. 4. For CTB_5 and CTB_5 + DTT, there was no significant difference between pH = 5 and pH = 8. Before activation of $CTAB_5$, population 2 had a slightly higher occupancy than at pH = 8 (81% vs. 75%) suggesting that at pH = 5 the A1 subunit had less disorder relative to the B_5 pentamer. After activation of $CTAB_5$, the percentage of population 2 dropped from 81% to 60%. This was less of a shift to population 1 compared to pH = 8.

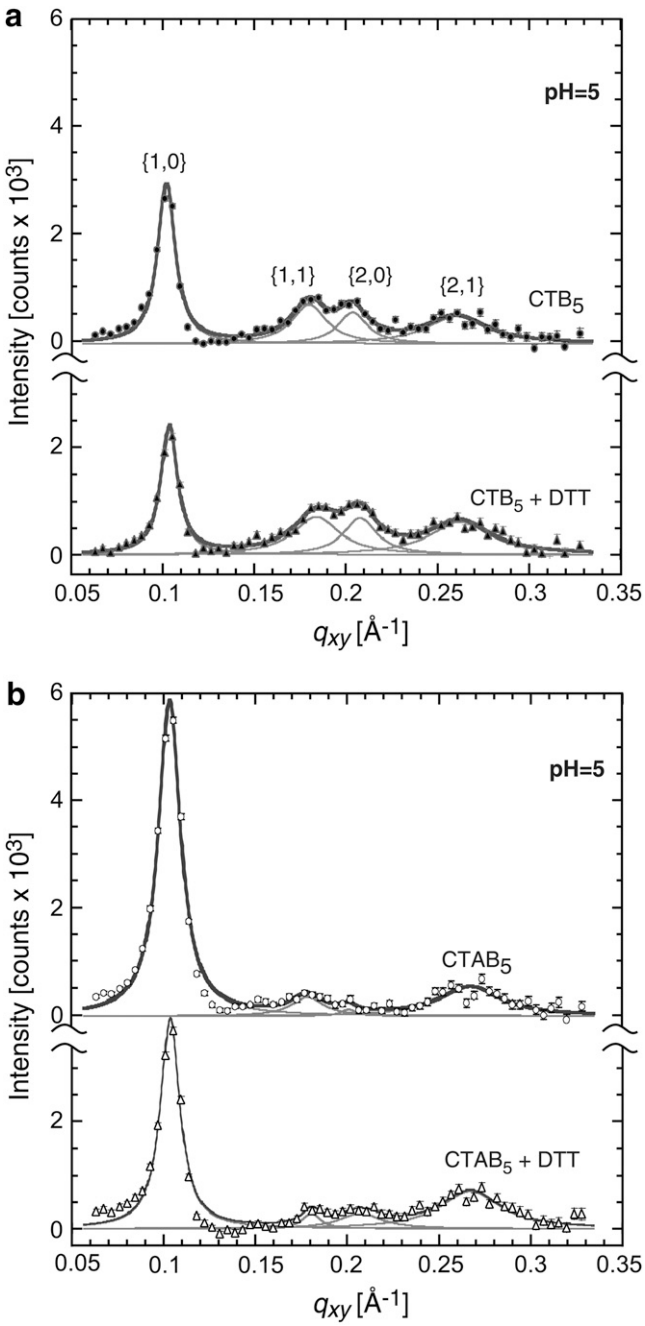

FIGURE 3 Grazing incidence x-ray diffraction (GIXD) Bragg peaks obtained for layers of CTB_5 and $CTAB_5$ with a subphase at pH = 5. The crystals nucleated on the DPPE:GM_1 monolayer forming an ordered 2D protein monolayer. The observed GIXD Bragg peaks indicate packing of the toxins in a hexagonal 2D unit cell. (*a*) Bragg peaks from CTB_5 and CTB_5 + DTT. Miller indices {h, k} of the observed peaks are indicated. Bragg peaks were integrated over the *qz* region from –0.05 to 0.2 $Å^{-1}$. Peaks were fitted (*solid lines*) using Lorenzian curves (see Table 1 for details). (*b*) Bragg peaks from $CTAB_5$ and $CTAB_5$ + DTT. Intensities and positions of the Bragg peaks (especially higher order) in the case of $CTAB_5$ had larger uncertainties due to weaker in-plane ordering and higher incoherent background contribution.

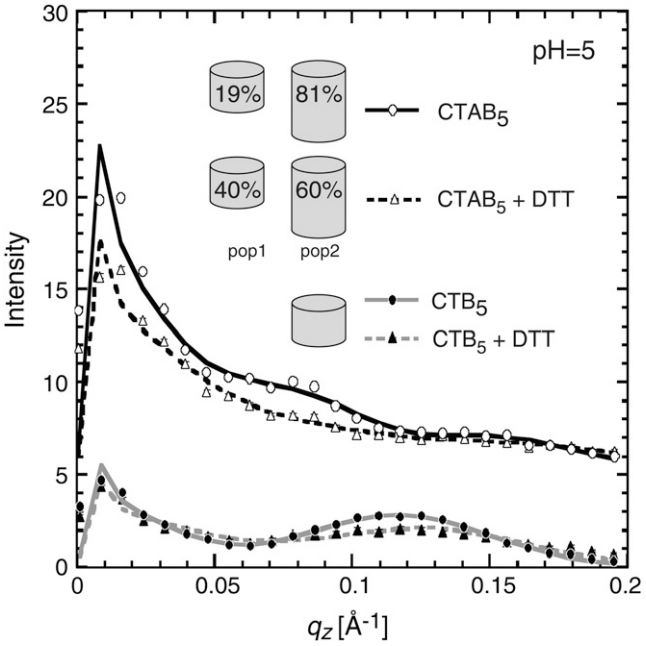

FIGURE 4 Bragg rod profiles corresponding to scattering from the cholera protein layer at pH = 5. Rods were produced by integrating through the 0.08 $Å^{-1} \leq q_{xy} \leq 0.12$ $Å^{-1}$ region of the {1,0} Bragg peaks in Fig. 3. Cylindrical objects were used to approximate the scattering units. Structural parameters such as the cylinder's height, radius, and tilt angle of the cholera molecules are reported in Table 2. In the case of $CTAB_5$, two populations of cylinders were used to fit the data. The curves corresponding to $CTAB_5$ have been offset for clarity. The sharp peak at $q_{xy} = 0.01Å^{-1}$ is the Vineyard-Yoneda peak (18).

CONCLUSIONS

Both CTB_5 and $CTAB_5$ crystallized into 2D clusters under the lipid monolayer with significant surface occupancy measured by x-ray reflectivity (Part I (14)). GIXD from the diffracting portion of the cholera toxin layer revealed a hexagonal unit cell ($a_{hex} \approx 71$–$74Å$ independent of pH) similar to EM studies ($a_{hex} \approx 68Å$) (11). Larger protein crystals as indicated by the in-plane coherence lengths were obtained at pH = 5. The largest protein cluster size was observed for CTB_5 (with and without DTT), and the smallest cluster size was with $CTAB_5$. In some cases, the protein-layer clusters were larger than the ordered lipid domain size (600Å vs. 400Å) (14). In all cases, addition of DTT caused an increase in lateral order, which was signified by increases in the L_{10} coherence length. Evidence for A subunit disulfide reduction by DTT came from two sources: GIXD from the protein layer and x-ray reflectivity of the lipid-protein system. X-ray reflectivity (Part I) showed that addition of DTT to $CTAB_5$ caused a decrease in the electron density in the A subunit region. Additionally, the intensity of the {1,0} reflection of the protein crystal layer was the largest in the case of $CTAB_5$ before activation because of electron contributions from the A subunit. After activation, the intensity of this peak decreased by ~38%. This was accompanied by a decrease in the percentage of the longer cylinders (population 2), which

were required to model the intensity distribution along the {1,0} Bragg rod. Simultaneous decreases in the DW factor after activation of $CTAB_5$ corroborated this observation, suggesting that the disulfide bond reduction of the A subunit diminished fluctuations of the protein normal to the surface and that the presence of the A subunit caused packing inefficiencies and greater disorder of the protein layer.

In summary, these studies revealed several key changes in the behavior of the cholera toxin-lipid system. Bragg rod analysis revealed a higher percentage of reduced A subunits at pH = 8, whereas pH = 5 favored the formation of larger-ordered domains. Finally, cleavage of disulfide bonds in $CTAB_5$ by DTT caused the greatest decrease in the in-plane coherence length of the lipid tail clusters at pH = 5. These findings suggest an enhancement of membrane penetration under low endosomal pH conditions.

We recognize Carlsberg, DanSync, Hamburger Synchrotronstrahlungslabor (HASYLAB) for beamtime and for the courage to judge the safety issues on their merits and allow these experiments to be performed. We thank Dr. Kristian Kjaer for help with the grazing incidence diffraction experiments.

The Los Alamos Neutron Science Center at the Los Alamos National Laboratory (LANL) is funded by the U.S. Department of Energy (DOE) under Contract W-7405-ENG-36. J.M and C.E.M. thank the LANL-Laboratory Directed Research and Development program, DOE Office of Science (Basic Energy Sciences) for financial support. C.E.M. acknowledges support from the LANL Director's Post-Doctoral Fellowship and the Institute for Complex Adaptive Matter. T.L.K. thanks the Jeff and Dianne Child/Steve Whitaker Fund for Distinguished Teaching and Scholarship for financial support.

REFERENCES

1. Haas, H., G. Brezesinski, and H. Mohwald. 1995. X-ray-diffraction of a protein crystal anchored at the air-water-interface. *Biophys. J.* 68: 312–314.
2. Lenne, P. F., B. Berge, A. Renault, C. Zakri, C. Venien-Bryan, S. Courty, F. Balavoine, W. Bergsma-Schutter, A. Brisson, G. Grubel, N. Boudet, O. Konovalov, and J. F. Legrand. 2000. Synchrotron radiation diffraction from two-dimensional protein crystals at the air/water interface. *Biophys. J.* 79:496–500.
3. Verclas, S. A. W., P. A. Howes, K. Kjaer, A. Wurlitzer, M. Weygand, G. Buldt, N. A. Dencher, and M. Losche. 1999. X-ray diffraction from a single layer of purple membrane at the air/water interface. *J. Mol. Biol.* 287:837–843.
4. Verclas, S. A. W., P. A. Howes, K. Kjaer, A. Wurlitzer, M. Weygand, G. Buldt, N. A. Dencher, and M. Losche. 1999. X-ray diffraction from a single layer of purple membrane at the air/water interface. *J. Mol. Biol.* 287:837–843.
5. Weygand, M., K. Kjaer, P. B. Howes, B. Wetzer, D. Pum, U. B. Sleytr, and M. Losche. 2002. Structural reorganization of phospholipid headgroups upon recrystallization of an S-layer lattice. *J. Phys. Chem. B.* 106:5793–5799.
6. Weygand, M., M. Schalke, P. B. Howes, K. Kjaer, J. Friedmann, B. Wetzer, D. Pum, U. B. Sleytr, and M. Losche. 2000. Coupling of protein sheet crystals (S-layers) to phospholipid monolayers. *J. Mater. Chem.* 10:141–148.
7. Weygand, M., B. Wetzer, D. Pum, U. B. Sleytr, N. Cuvillier, K. Kjaer, P. B. Howes, and M. Losche. 1999. Bacterial S-layer protein coupling to lipids: x-ray reflectivity and grazing incidence diffraction studies. *Biophys. J.* 76:458–468.
8. Jensen, T. R., K. Balashev, T. Bjornholm, and K. Kjaer. 2001. Novel methods for studying lipids and lipases and their mutual interaction at interfaces. Part II. Surface sensitive synchrotron x-ray scattering. *Biochimie.* 83:399–408.
9. Als-Nielsen, J., D. Jacquemain, K. Kjaer, F. Leveiller, M. Lahav, and L. Leiserowitz. 1994. Principles and applications of grazing incidence x-ray and neutron scattering from ordered molecular monolayers at the air-water interface. *Phys. Rep.* 246:252–313 [review].
10. Ludwig, D. S., H. O. Ribi, G. K. Schoolnik, and R. D. Kornberg. 1986. Two-dimensional crystals of cholera-toxin b-subunit receptor complexes - projected structure at 17-a resolution. *Proc. Natl. Acad. Sci. USA.* 83:8585–8588.
11. Mosser, G., V. Mallouh, and A. Brisson. 1992. A 9 angstrom 2-dimensional projected structure of cholera-toxin b-subunit-g(m1) complexes determined by electron crystallography. *J. Mol. Biol.* 226: 23–28.
12. Zhang, R. G., M. L. Westbrook, E. M. Westbrook, D. L. Scott, Z. Otwinowski, P. R. Maulik, R. A. Reed, and G. G. Shipley. 1995. The 2.4 angstrom crystal structure of cholera toxin b subunit pentamer - choleragenoid. *J. Mol. Biol.* 251:550–562.
13. Ribi, H. O., D. S. Ludwig, K. L. Mercer, G. K. Schoolnik, and R. D. Kornberg. 1988. 3-dimensional structure of cholera-toxin penetrating a lipid-membrane. *Science.* 239:1272–1276.
14. Miller, C. E., J. Majewski, E. B. Watkins, and T. L. Kuhl. 2007. Part I: an x-ray scattering study of cholera toxin binding, penetration, and induced phase transformations in lipid membranes. *Biophys. J.* 95:629–640.
15. Als-Nielsen, J., and K. Kjaer. 1989. X-ray reflectivity and diffraction studies of liquid surfaces and surfactant monolayers. *In* T. Riste and D. Sherrington, editors. Plenum Press, Geilo, Norway. 113–137.
16. Kjaer, K. 1994. Some simple ideas on x-ray reflection and grazing-incidence diffraction from thin surfactant films. *Physica B.* 198:100–109.
17. Guinier, A. 1963. X-Ray Diffraction in Crystals, Imperfect Crystals, and Amorphous Bodies. W. H. Freeman, San Francisco.
18. Vineyard, G. H. 1982. Grazing-incidence diffraction and the distorted-wave approximation for the study of surfaces. *Phys. Rev. B.* 26:4146–4159.